

# A Short-range Ship Navigation System based on Ladar Imaging and Target Tracking for Improved Safety and Efficiency

Antonio R. Jiménez and Fernando Seco

## Abstract

A new maritime navigation system based on a laser range-finder scanner for obstacle avoidance and precise maneuvering operations is described in this paper. The main novelty of this work is the adaptation and implementation of known technology for laser range-finding and algorithms for target tracking, into a system that operates in real-time and has been tested in different natural sea and in-land navigation scenarios. The principal components of this system: the laser range-finder, the scanning unit and the data processing and displaying unit, are described in detail. Ladar images are dense in the horizontal direction and sparse vertically as a compromise between capturing relevant features and quick frame formation. Images are processed for range outlier removal and significant observable patterns are extracted. This multi-target tracking problem is tackled using robust Kalman filtering techniques for a continuous tracking of each detected observation. We minimize unreliable track initializations and preserve tracks from deletion during temporal mis-observations. The evaluation in open-sea and in-land waterways gave good results, making the system valid for precise maneuvering, fluent navigation and accident mitigation. Objects of interest, from boats to ships, are detected and robustly tracked; pier and lock chamber sketches are reliable; bridge height estimation is precise; and narrow waterways (river banks and bridge columns) are correctly detected. The prototype developed can be considered as a very valuable complementary device to traditional radar-based techniques, that are not totally valid for accurate short-range exploration, improving the efficiency and safety in ship operations.

## Index Terms

Maritime and Inland Navigation, Safety and Collision Avoidance, Efficient Intelligent Navigation, LADAR, Image processing and de-noising, Kalman filtering, Multiple target tracking, Observation-to-track association, Integrating GPS/ECDIS with LADAR.

## I. INTRODUCTION

**M**ODERN ships are equipped with sophisticated navigation aids [1] mainly devoted to vessel positioning, efficient communication, and the exploration of the environment. Location devices determine the position and orientation of the ship with respect to a map; they include GPS, Loran, and the Electronic Chart Display and Information System (ECDIS). Telecommunication systems like the Global Maritime Distress and Safety System (GMDSS) or the Automatic Identification System (AIS) are useful for communication with the Vessel Traffic Service (VTS) or with other neighboring ships. Exploration devices like radar and depth sounders are useful to explore the surroundings of the vessel.

Nowadays, in ports with a high density of vessels, ship coordination is managed by a VTS, which assigns a time-slot for each vessel and gives directions for safe navigation. Nevertheless, in some situations an approaching vessel can enter the VTS radio-controlled zone out of schedule or without permission [2], [3], a circumstance under which the existing aids might not be sufficient to avoid collisions. In in-land waterways (rivers and canals) the density of ships navigating in narrow passageways, surrounded by many small objects, and the need of executing diverse manoeuvres, create a risky scenario for accidents and collisions that a maritime radar can not always detect.

Safety and efficiency problems are found in many accurate sailing maneuvers such as entering/leaving the port, berthing/clearing the pier for the maritime operation, overtaking slower vessels in narrow channels, passing between the columns of a bridge, passing under a bridge with critical height, entering/leaving the lock chamber quickly, or coupling with other vessels [4]. A couple of these situations are illustrated in

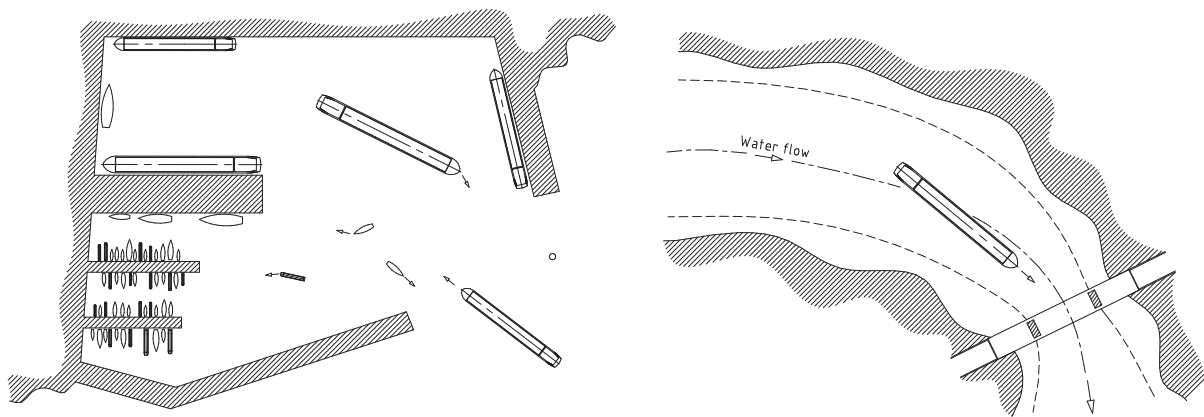


Fig. 1. Two common situations where navigation aids are useful: (left) entering the port and berthing the pier; (right) river navigation passing through narrow bridge columns

figure 1. These maneuvers are performed slowly and inefficiently, closely supervised by crew members in order to avoid collisions.

European statistics [4] show that, for inland waterways, ship-to-ship or ship-to-fixed-object collisions account for nearly 50% of all accidents, and surprisingly they tend to happen in good visibility conditions. Furthermore, in 35% of collisions, the dangerous situation of the ship was noticed too late, while, for 40% of the cases, it went unperceived until the collision. Although most of the existing data considers only large vessels, some studies [5] have shown even higher number of accidents for small vessels, leisure and high speed crafts. The consequences of these accidents, in the form of human casualties, environmental disasters and economic losses, are a strong motivation for the development and improvement of existing navigation aids.

Radar (RADio Detection And Ranging) is the standard sensor for detection of obstacles or ships in maritime navigation, operating by measuring the time taken by a radio signal to travel from a ship to the obstacle and back [6], [7]. Most obstacles produce a strong reflection of the radar signal, permitting the estimation of their range and bearing. Depending on the application, different radio frequencies are chosen, and therefore different wavelengths, patterns of emission, and lateral resolution are achieved. Band HF (3-30 MHz) is used for coastal radar systems; band L (1-2 GHz) for long-range air traffic control; band X (8-12 GHz) is used for marine radar and missile guidance; and the W band (75-110 GHz; 4 mm wavelength) is used as a high resolution sensor for autonomous vehicles.

Lateral resolution for fixed-beam radars, or mechanically-scanning antennas, is limited by the beam divergence (beamwidth), which for currently-available maritime slotted waveguide antennas at 9.4 GHz, is typically about 1 degree in the horizontal direction (a 10 meter spot diameter at 500 meter range). No vertical information is captured since vertical beamwidth is large (20 degrees or more). Electronic scanning phased arrays achieve high axial and lateral resolutions without mechanical movement, but have a limited field of view and high cost [8].

The typical measuring range of a maritime radar is between 0.3 and 3-5 km. Short-range radars (range from a few to 150 meters) have been designed using pulsed compression techniques to augment the axial resolution of traditional radars while maintaining a constant transmitted energy level. These short-range radars have been used for Automatic Cruise Control (ACC) of cars at the 77 GHz W band or the 24 GHz E band [9], [10], [11]; however, in spite of an increased axial resolution, the lateral resolution is poor, and the horizontal radiation pattern (less than 15 degrees) is too narrow for maritime applications.

For accident mitigation and precise manoeuvring it would be desirable a radar-like exploration instrument capable of operating at short ranges (0 to 500 meters), with good axial and lateral resolution, being robust against clutter, and having a wide and adaptive field of view. Existing radar technology can not be used for close obstacle avoidance and precise manoeuvring since it does not yet fulfill above-cited

requirements [12].

LIDAR (Light Detection And Ranging) is a distance measurement technique similar to radar technology, which uses light instead of radio [13]. As the source of light is typically a Laser, Lidar is also known as LADAR (LAsER Detection And Ranging), and in military contexts with the misleading term *laser radar*. Because the beam divergence of a laser is proportional to the ratio wavelength/beam diameter at the transmitter, ladars are much more collimated than RF radars (typical laser beam divergence about 1 mrad); moreover, the emitting profile of a laser is typically Gaussian and free of side lobes; consequently, very high lateral resolution can be achieved. Besides, axial resolution can be as high as one millimeter for most reflecting surfaces. Therefore, it is possible to image any type of object (even of reduced dimensions), and made of almost any material (except for mirror-like surfaces or black-painted objects), many of which would be invisible at radar frequencies.

A disadvantage of current ladar technology is the time needed for the completion of an image; in real time operation a tradeoff must be established between update rate and resolution (number of line scans per frame). Next generation of ladars will reduce this acquisition time by using scannerless Focal Plane Array (FPA) [14]. Compared with radiofrequency, laser radiation is scattered by aerosols and cloud particles, which can limit its operating range. Signal processing techniques have been developed to detect object of interest even in poor visibility conditions [15].

Classical applications of ladars include detection of the presence of particles and contaminants in the atmosphere, satellite distance measurement, traffic speed law enforcement in highly-dense conditions, or identification of tanks using ladar imaging. New applications of Ladars include research projects for increasing safety in road transport [16] and autonomously guided ground vehicles [17]; a notorious example is the DARPA Grand Challenge contest [18].

This paper deals with the development and testing of a new short-range LADAR tracking system intended for efficient and safe navigation in rivers, canals and sea. The paper will address the design of the laser scanner system, and the tasks of image acquisition, pattern identification and tracking of obstacles. Results of tests of the prototype in open-sea and inland waterways will also be given.

## II. OBJECTIVES AND SYSTEMS REQUIREMENTS

The goal of the proposed Ladar system is to serve as a navigation aid for more efficient water transport and avoidance of accidents (by triggering alarms or even actuating automatically on skipper controls). It must be operative in the short range (0 to 500 meters), have high enough lateral and axial resolution, and a wide and dynamic field of view necessary for the common close range manoeuvres. It should also be operative 24 hours a day, and even in adverse weather conditions (fog or rain). The system must be designed for fully integration with other devices already present in the ship (GPS, radar, etc).

Table I gives the quantitative requirements that a precise ranging navigation sensor should fulfil to cope with common operations, both in open sea and inland navigation. These requirements include maximum range, field of view (FOV) and range accuracy. This table is based in studies done by the German Development Center for Ship Technology and Transport Systems (DST) [19], and serves as a design guide for our system.

We restrict the operating range of our sensor to 500 m, which covers all in-land navigation operations and the maritime maneuvers close to the pier. A ranging accuracy of 0.1 m is enough for these operations. The Ladar should have a panoramic horizontal field of view (covering at least 180 degrees in front of the ship), and a 90 degree vertical view (between 5 degrees above the horizon and 85 degrees downward). However, this field of view should be configurable during operation, in order to optimize the time of capture for each of the ship operation modes listed in table I.

According to DST Center [19], the update frequency needed for most maneuvers in table I is 1 Hz. This estimation takes into account the skipper's reaction time, the ship dynamics, and the proximity to the obstacle. However, other critical short-range operations, such as, berthing/leaving the pier, locking, or coupling with others ships, requires update frequencies as high as 10 Hz, specially if an automatic maneuver must be implemented.

TABLE I  
SENSOR REQUIREMENTS FOR VARIOUS SHIP MANOEUVRES (BASED ON [19])

Ship operation	Maximum range (m)	horizontal FOV (°)	Vertical FOV (°)	Range accuracy (m)
Maritime field				
Open sea navigation	1000	[-30,30]	[0,-10]	10
Entering/Leaving the port	1000	[-90,90]	[0,-45]	1
Berthing/Clearing the pier	100	[0,90]	[0,-85]	0.1
Mooring to the buoy	300	[-90,90]	[0,-45]	0.1
Inland navigation				
By-passing other vessel	500	[-30,30]	[0,-30]	1
Overtaking other vessel	500	[-30,30]	[0,-30]	1
Passing between columns	500	[-90,90]	0	1
Passing under the bridge	500	[-5,5]	[5,-5]	0.1
Entering/Leaving the port	500	[-90,90]	[0,-45]	1
Berthing/Clearing the pier	100	[0,90]	[0,-85]	0.1
Locking	100	[0,90]	[0,-85]	0.1
Coupling with other ship	100	[0,90]	[0,-85]	0.1

The raw Ladar data will be processed to identify obstacles or objects of interest (like the wall of the pier, other ships, etc). These objects should be tracked, using multiple-target tracking techniques based on Kalman filtering [20], [21], to continuously update their pose and course information, which could be used to provide a quantitative and symbolic representation on an alphanumeric and graphical display.

### III. THE LADAR NAVIGATION SYSTEM

The Ladar system proposed in this paper consists basically of two main elements: 1) the Ladar imaging system (including the laser range-finder and the scanner) and 2) a target tracking processing unit with a man-machine interface (MMI) (see figure 2). A NMEA multiplexer is used to communicate external equipment with the processing unit.

#### A. The ranging module

The ranging module is the central element of the ladar system. It consists of a diode-pumped Nd:YAG infrared laser emitter provided by Nanolase, with a wavelength  $\lambda = 1.064 \mu\text{m}$ , Gaussian pulse shape with a temporal duration of 1.5 ns, and a 15 kHz pulse repetition rate. The laser beam profile corresponds to the fundamental traverse (Gaussian) mode, and, after being expanded by a collimator lens upon emerging from the emitter, has a waist radius of 14.5 mm and beam divergence of 1.5 mrad (the typical spot size at a 100 m range is 0.3 m). Although the peak power of the laser is high ( $P_t = 1 \text{ kW}$ ), the short pulse length causes an average emitted power of only 22.5 mW, which falls within the regulated Accepted Emission Limits (AEL) [15]. The design of the ranging module is compliant with Class I eye-safety regulations, and poses no problems to people situated in the scanning area.

When obstacles are found in the path of the ray, part of the emitted energy is reflected back to the ship and received by a photodetector placed close to the laser source. An InGaAs APD (avalanche photodiode) from EG&G, with a power detection threshold of 53 nW is used for that purpose. The SNR of the process is enhanced by an interference filter (IF) placed before the APD, with a bandpass window around the central laser wavelength (1064 nm) of  $\pm 2 \text{ nm}$ , reducing the solar radiation to 11.7 nW.

The optical power  $P_r$  returned by an obstacle at a distance  $R$  from the emitter is given by the, so called, *laser radar equation* [13]:

$$P_r = P_t T_o e^{-2\sigma R} \frac{\rho A_r}{\pi R^2}, \quad (1)$$

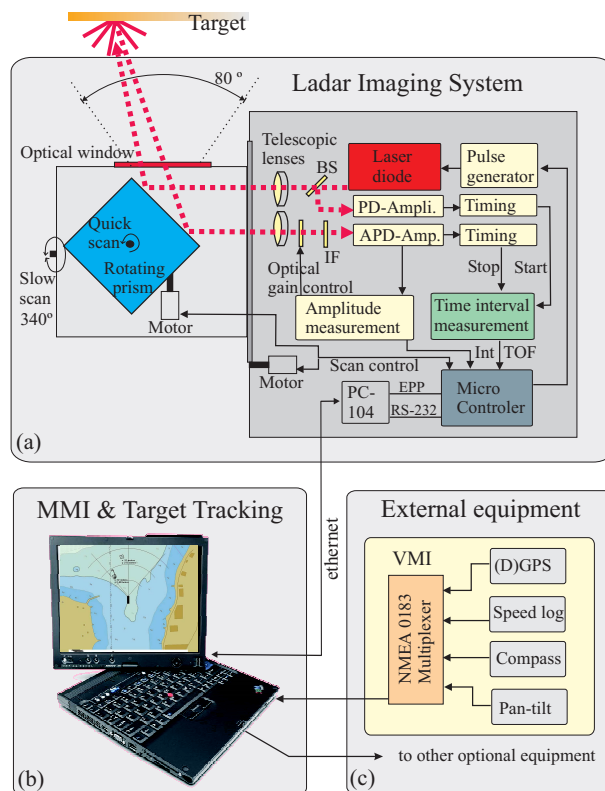


Fig. 2. Block diagram of the short-range Ladar system: (a) the Ladar imaging system including main optical components, electronic inter-connections, and the physical layout of mechanical components; (b) central processing unit for detection, tracking and user interface; (c) connection with some needed external vessel equipments (an optional output could be provided to disseminate Ladar information).

where  $P_t$  is the laser output power,  $T_o$  is the transmission coefficient of the emitting and receiving optics,  $\rho$  is the reflectance of target surface,  $A_r$  is the area of the receiver optics, and Lambertian reflectance is assumed, so the received power does not depend on the relative orientation of the reflector. The power decay caused by propagation of the laser signal through the atmosphere (traversed length  $2R$ ) is modelled by the Beer-Lambert law [22], [23] (exponential term in eq. 1). The value of the attenuation coefficient,  $\sigma$ , is dependent on the conditions of the atmosphere and the physical mechanisms causing the scattering. Mie scattering dominates in situations of haze and fog where the particle size ( $0.01\text{-}20\ \mu\text{m}$ ) is comparable to the wavelength of the laser, while for bigger particles (rain, snow or hail), geometrical scattering, approximately independent of the wavelength, takes place. Typical values for the attenuation coefficient  $\sigma$  are: 0.1 for clear air, 1 for haze and 10 for fog [24], which represent transmission losses of 0.43, 4.3 and 43 dB/km, respectively.

Considering equation 1 for a target of reflectance  $\rho = 0.3$ , a sensor area  $A_r$  of  $13\ \text{cm}^2$ , and an optical transmission coefficient  $T_o$  of 0.49, then a maximum detection range of 1000 m would be theoretically obtainable in clear conditions (visibility of 15 km). This would be reduced to 600 m in hazy days (visibility of 2 Km), or 300 m when fog was present (visibility of 300 m). However, these are theoretical predictions based on equation 1. Some basic ranging tests performed with our laser ranging module, in clear conditions, showed that the maximum achievable measuring distance was about 500 meters (using typical objects present in several natural scenarios). So the empirical maximum ranging distance is half of the expected by theoretical calculus (500 m instead of 1000 m). The ranging discrepancies between theoretical and experimental results can be attributed to the fact that the laser radar equation considers a perfectly Lambertian surface, however in a real scenario surfaces are not totally diffusive and have a specular behavior that causes less energy reflected back to the laser receiver.

We also tested the ranging accuracy in clear visibility conditions using artificial targets (circular panels

of 0.75 meter radius with a reflectance  $\rho = 0.3$ ). Capturing a long sequence of range readings at several distances (100, 300 and 500 meters) the accuracy for the worst case corresponding to the maximum distance (500 m) was 0.11 m with a 95% confidence level (i.e. only 5% of measurements were larger than 0.11 m).

An additional problem could take place when the fog is dense enough, causing a laser reflection, which could be misinterpreted as an obstacle. However, the timing signal processing unit is capable of identifying several echoes, such as the long and dispersed pulse coming from the fog, and those reflections coming from the target itself. It permits to eliminate the first one coming from the dense fog, taking only into account the echoes from objects that are much more time-compressed (sharp). Some ranging tests performed with the ranging module, in foggy conditions (300 meters visibility), showed that the maximum achievable measuring distance was about 250 meters in a natural scenario. In this case, the empirical maximum ranging distance in foggy conditions (300 m) is quite similar to the obtained in real test (250 m). The maximum ranging capability of the Ladar system, obtained by experimentation in clear and foggy conditions, are summarized in table II.

### B. The scanner

The function of the scanner is to deflect the laser beam in order to form an image which describes the scene in front of the ship. There are several approaches for this purpose [25]. The acousto- and electro-optical effects, which change the refraction index of certain materials by applying acoustic and electric fields, respectively, have been used to deflect light in a controlled way, but the maximum angles available with current technology (under  $3^\circ$ ) are too limited for our purposes.

Reflective scanning is achieved by mechanically changing the orientation of a mirror. Piezoelectric motors limit the maximum angle of excursion (below 1-2 degrees). But galvanometric motors, with very high positioning accuracy (about  $10 \mu\text{rad}$ ), high speed ( $>500$  lines/s), and wide excursion angles (60 degrees), are a practical solution for scanning a scene by moving a couple of low-inertia mirrors [26]. These scanners meant for real time operation have to achieve a compromise between the density of points of the image and the time taken to complete a full scene scan; for example, acquisition of a high density image ( $600 \times 600$  pixels) may require more than 10 s.

The requisites for our system are a maximum acquisition time of 1 s for a complete image frame, and enough pixel density of the ladar image to guarantee the detectability of objects of interest.

We have used a scanner from the company Riegl (model LMS-Z210), placed at the bow of the ship as shown in figure 3. The scanner consists of a cube with specular sides rotating at a constant angular speed around a vertical axis, which deflects the laser beam in the horizontal plane, covering a total range of  $80^\circ$ . Acquisition of a single line takes 200 ms, but out of the 3000 laser emissions which take place in that interval, half are lost during the transition between the sides of the cube; in consequence, a single horizontal line has 1500 points. The rotating prism can also be slowly revolved around the horizontal axis to perform a vertical scan; the angular range in this direction is higher ( $340^\circ$ ), but the speed is limited to a maximum  $15^\circ\text{s}^{-1}$ . In consequence, a complete image frame consists of a few (1–10 lines) horizontal lines, each of about 1500 range points, and takes between 0.2 and 2 s to be acquired.

Horizontal resolution of the ladar is very high, with consecutive points being separated by only 0.9 mrad, which is less than the beam divergence (1.5 mrad), so there is some point overlap. The area illuminated by the laser at a range of 100 m is a circle of diameter 0.3 m, which will detect most objects relevant to the security of the vessel. However, gaps between the horizontal lines of a frame can exist; at the maximum speed of  $15^\circ/\text{s}$  for the slow scanning axis, these angular gaps can be as large as 3 degrees. Fortunately, this limitation is not critical thanks to the oscillatory motion of the ship that produces a natural spread of the horizontal lines, filling the horizontal gaps present in a static acquisition.

In the maritime field the rolling and pitching rotatory oscillations, as well as the heaving (vertical translational oscillation), are very significant. The amplitude and frequencies of these motions depends on sea-state, heading and speed of the ship in relation to the waves, size of the ship, shape of the hull



Fig. 3. Picture of the ladar system on the bow of a vessel in navigation trials.

Horizontal scan range	80 deg
Time to complete a horizontal scan	200 ms
Vertical scan range	340 deg
Angular vertical scan speed	15 deg/s
Beam divergence	1.5 mrad
Spot diameter at 100 m distance	0.3 meters
Max. range (clear: 15 km visibility)	500 m
Max. range (fog: 300 m visibility)	250 m
Minimum measuring distance	1 m
Frame acquisition time	1 s (5 vertical lines)
Protection class of the ladar head	IP64

TABLE II

OBTAINED TECHNICAL SPECIFICATIONS OF LADAR.

and positions of ship's center of gravity and center of buoyancy. For passenger ferries a typical angle of heel (maximum rolling amplitude) can be about 8 degrees, and the rolling period is usually between 8 and 15 seconds (typical design compromise between stability and comfortability). The consequence is that the detection capability of the ladar could be increased by the vessel oscillation after fusing a few consecutive frames (about 10 frames for a typical rolling period).

The most important performance parameters of the laser scanner, as well as the achievable distance measurements with the ranging unit, are listed in table II.

### C. Ladar image formation

We added an actuator to rotate the scanner by  $90^\circ$  and to interchange the horizontal and vertical axes. The purpose was to achieve maximum flexibility during scene scanning, specially to cope with most field of view requirements during manoeuvring.

In principle, interchanging the horizontal and vertical axes (dense lines vertically), makes possible to cover all field of view requirements, listed in table I, for every mode of operation. This scanning mode can achieve horizontal panoramic view ( $\pm 90^\circ$ ) while exploring  $80^\circ$  vertically below the horizon. However, simulation analysis indicate that it is not optimum for obstacle detection at distances above 100 meters, since most range values are wasted scanning the sky and specially down the sea. The fixed  $80^\circ$  vertical scanning is too large for long ranges, and therefore a lower scanning range will suffice. Additionally, the acquisition of this  $\pm 90^\circ$  panoramic-view frame requires about 12 seconds, and consequently the vessel speed must be very low for these precise maneuvers.

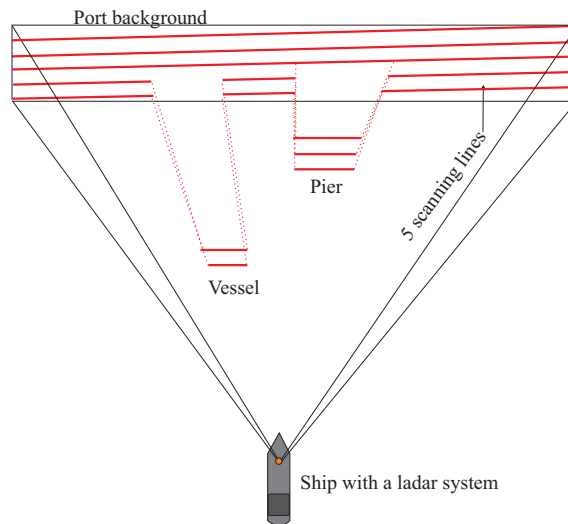


Fig. 4. Default raw Ladar image acquisition. Five lines are registered using fast scanning horizontally. It represents an ideal acquisition where a ship is approaching a port (larger ranges at the background), and a vessel and the pier is being detected (shorter ranges).

On the contrary, the fast horizontal scanning mode with few dense lines (see fig. 4), makes it possible to maximize the number of valid and representative range values. For their benefits, this will be the default scanning mode for image acquisition. The acquisition mode will be switched to dense vertical scanning ( $90^\circ$  scanner rotation) only if a high angular resolution is needed, such as in bridge height measurement, or in manoeuvres needing a panoramic view (entering/leaving small ports).

#### D. Vessel-machine and man-machine interfaces

The Ladar imaging system described above is connected to a PC onboard of the ship using an ethernet link. A vessel-machine Interface (VMI) has been built to retrieve additional information from others navigation sensors such as DGPS, the speed log and (gyro)compass. This data is needed to correctly match the ladar readings with the stored ECDIS maps and determine the ship's position and orientation. Moreover, via the VMI, the ladar system can provide useful information to other navigation devices already installed on the ship (autopilot module, dynamic positioning system, sonar, radar, etc).

The man-machine interface (MMI) provides visual information to the skipper, by presenting the ladar readings on top of an ECDIS map. After processing the raw ladar data, potential threats (other ships, bridges, etc) can be tracked and displayed on the computer screen. This topic is treated with more detail in the next section.

## IV. METHODS FOR OBSTACLE IDENTIFICATION AND TRACKING

A raw Ladar representation (polar range plot) is very useful for a skipper but sometimes difficult to interpret. A reliable methodology for obstacle identification and tracking is very important to automatically detect significant targets in the surroundings and to highlight those objects on the pilot's Ladar screen. Additionally, target tracking is essential for creating intelligent navigation aids, which could be used for real-time ship automatic control in collision avoidance or precise manoeuvring.

We have used, and adapted to our particular Ladar navigation problem, modern multiple-target tracking (MTT) techniques [27] to automatically detect and track targets of interest while removing clutter.

Our developed software is represented and modelled in figure 5 using a standard *Data Flow Diagram* (DFD) [28]. A data flow model represents the flow of data between external entities, processes, and data stores. Processes are functions that get some input data (represented by an incoming arrow), process the information by the execution of some algorithms, and finally generate some results (outgoing arrow). Our two main processing blocks are represented in figure 5: 1) Detection - Ladar image processing and pattern

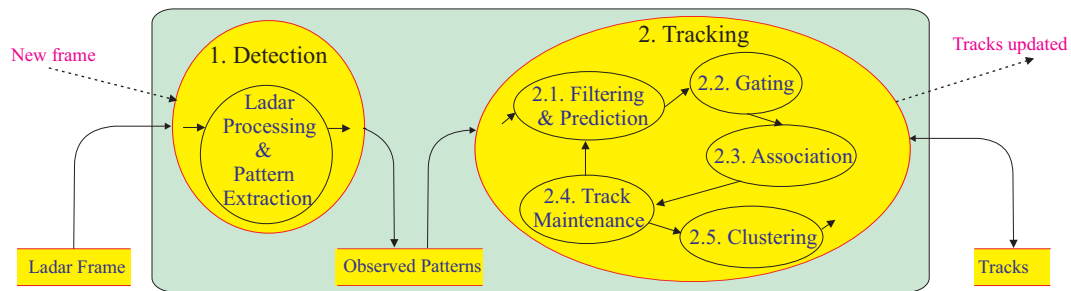


Fig. 5. Data Flow Diagram (DFD) modelling the whole target identification and tracking process. Bubbles represent Ladar image processing algorithms, rectangular boxes contain the processed data, solid-line arrows indicate the data flow, and dashed-line arrows are control messages to/from a higher-level software.

extraction (transforms *Ladar frames* into *observed patterns*), 2) Target tracking (uses *observed patterns* and generates *target tracks*). This *tracking* processing block is also modelled as the interaction of other processes: 2.1) State filtering and motion prediction), 2.2) Gating, 2.3) Observation-to-Track Association, 2.4) Maintenance for track creation and deletion, and 2.5) Clustering of multiple tracks. Next subsections give details on the implementation of these processes for our particular problem.

#### A. Ladar image processing and extraction of patterns

The goal of this processing block (left bubble in fig.5) is the detection of *patterns* of interest in background noise by analyzing each acquired Ladar frame. A *pattern* is any observable feature in one Ladar range profile characterized by a smooth section limited by two sharp edges at each of its sides (for example, almost any individual object, within a 500 m distance from the scanner, causes at least one smooth range section with a discontinuity at each sides defined by the width of the object). In this *pattern* extraction process, it is necessary to diminish background noise due to unreliable laser reflections or partitioned range profiles due to mis-reflections. The proposed Ladar image processing begins with a de-noising stage for outlier removal, followed by a segmentation process to separate possible *patterns* of interest from the background.

The de-noising process uses robust filtering techniques (median filters) to remove outliers from the range profiles [29], [30], [31], [32]. The selection of the size of median buffers is a trade-off between noise reduction efficiency and angular resolution. We selected a buffer size of 7, which keeps resolution below 0.6 meters (at 100 m distance) and removes most erroneous discontinuities on smooth surfaces.

During segmentation, the discontinuities at both sides of a smooth range section define the limits of the *pattern* of interest. These discontinuities are detected with the Canny operator [33] which is used extensively in image edge-detection. Given the non-perfectly continuous surface or reflectance of some objects, and the centimeter range resolution of the Ladar, most detected objects generate not one but multiple *patterns*. For example, as the laser scans over the surface of a ship, discontinuities in the measured range are very often produced as it travels from the hull to the bridge and then the deck, caused by the different geometry of these parts or even changes in the reflectivity. After a full frame acquisition, a list of the observed patterns, with their size, range and orientation angle, are passed to the next tracking stage (right bubble in fig.5) devoted to target state estimation, to check if they actually belong to the same physical object, or are rather caused by temporal coincidence (for example, two ships passing close by). This estimation and association procedure is described in next sections.

#### B. Filtering and prediction for track motion estimation

Observed *patterns*, resulting from the previous Ladar processing stage, are the *observations* that feed the state prediction stage for kinematics motion estimation. A state associated to the motion of a persistent observation is called for simplicity a *track*. The classical Kalman filtering formulation for recursive least square estimation (RLSE) is used for track kinematics estimation [34].

In order to uncouple range and angular estimations, and to avoid virtual accelerations appearing in range and angles when a target is moving at constant velocity along a straight line in a cartesian reference frame, then our range and angular observations  $(r, \theta, \phi)$  are transformed to cartesian coordinates  $(x, y, z)$  before applying the Kalman filtering. The cartesian coordinate system that we use is referenced and fixed to the laser scanner, which normally is at the bow of the ship.

Three independent Kalman filters are used to estimate each 1-D cartesian component  $(x, y, z)$  of each target under track. For the one dimensional  $x$  component, at sample  $i$ , the state will be denoted by  $\mathbf{a}_i = (x, \dot{x})$ , and the observation at that time along x-axis is a scalar denoted by  $b_i$ , and related to current state by this *measurement model*:

$$b_i = \mathbf{H} \cdot \mathbf{a}_i + v_i, \quad (2)$$

where  $\mathbf{H}$  is the measurement matrix ( $\mathbf{H} = [1, 0]$  in our case), and  $v_i$  is the zero-mean Gaussian measurement noise with covariance  $R$ . Matrix  $R$  is a scalar in our case and depends non-linearly on the actual range  $r$ , azimuth  $\theta$ , and Ladar acquisition noise for azimuth  $\sigma_\theta$  and range  $\sigma_r$  [27]. For  $\theta = 40^\circ$ ,  $r = 150$  m,  $\sigma_\theta = 0.01$  rad, and  $\sigma_r = 0.1$  m,  $R$  is evaluated as follows:

$$R = [\sigma_x^2] = [\sigma_r^2 \cos^2 \theta + \sigma_\theta^2 r^2 \sin^2 \theta] \simeq 1. \quad (3)$$

We use a Singer acceleration model to represent the *motion model*, which for sample intervals,  $T$ , similar to the Singer time constant  $\tau_m$  (both about 1 second), degenerates into a constant velocity dynamic model [20], [27]. This constant velocity *motion model* it is very valuable for its better filtering performance, when the derivatives of parameters to estimate are not available via measurement. This constant velocity model provides position estimations with low variance, although lags could be increased in some high-accelerating maneuvers [27]. The state transition matrix  $\Phi$  for the constant velocity model is:

$$\Phi = \begin{pmatrix} 1 & T \\ 0 & 1 \end{pmatrix}. \quad (4)$$

The sampling interval,  $T$ , equals the Ladar frame update rate that is 1 second for the default acquisition mode.

Using this motion model, the state *prediction*  $\mathbf{a}_{i+1,i}$  (needed to center the gating window during association) is calculated from the previous filtered state  $\mathbf{a}_{i,i}$ , with the *prediction equation* as follows:

$$\mathbf{a}_{i+1,i} = \Phi \cdot \mathbf{a}_{i,i} + \mathbf{q}_i, \quad (5)$$

where  $\mathbf{q}_i$  is the *motion* noise with covariance  $\mathbf{Q}$ , which models the randomness in the position and velocity of the target around the predicted next state. Note that the positioning error includes in our case, not only the random accelerations and maneuvers of tracked target, but also those random motion changes at the ship equipped with the Laser system (waves move ship randomly in heading and rolling). The Singer acceleration model representing *motion* noise, when  $\tau_m \simeq T = 1$  second, degenerates into a zero-mean white Gaussian constant velocity dynamic model [20], [27], that for  $\sigma_{x0}^2 = 1$  meters, can be expressed as

$$\mathbf{Q} = 10 \cdot \sigma_{x0}^2 \cdot \begin{pmatrix} T^3/3 & T^2/2 \\ T^2/2 & T \end{pmatrix} = \begin{pmatrix} 3.3 & 5 \\ 5 & 10 \end{pmatrix}. \quad (6)$$

After a prediction and a new measurement, the refined target state at sample  $i$ ,  $\mathbf{a}_{i,i}$ , is given by the *filtering equation* [20]:

$$\mathbf{a}_{i,i} = \mathbf{a}_{i,i-1} + \mathbf{k}_i [b_i - \mathbf{H} \cdot \Phi \cdot \mathbf{a}_{i-1,i-1}] \quad (7)$$

The covariance matrix of state estimations,  $\mathbf{P}$ , provides an indication of the quality of estimations, and therefore we use it to define the *gate* (size of the window around target's predicted position) during the

observation-to-track MTT association problem. The initial value ( $i=0$ ) for the covariance matrix  $\mathbf{P}$ , for  $\sigma_{x0}^2 = 1$  m and  $\sigma_{v_{x0}}^2 = 5$  m/s, was

$$\mathbf{P}_0 = \begin{pmatrix} \sigma_{x0}^2 & 0 \\ 0 & \sigma_{v_{x0}}^2 \end{pmatrix} = \begin{pmatrix} 1 & 0 \\ 0 & 25 \end{pmatrix}. \quad (8)$$

### C. Gating and Observation-to-Track Association

Association in multiple-target tracking is one of the most challenging tasks. It consists in simultaneously matching several observations to several tracks in an optimum manner [35]. We start data association with a *gating test* that must be fulfilled to determine which observations are valid candidates to update existing tracks. To define the center of the gate we use the predicted 2-D position of a track  $(\hat{x}, \hat{y})$  obtained using the Kalman positioning predictions,  $\mathbf{a}_{i+1,i}$ , available from (5) for the  $x$ - and  $y$ -axis.

A normalized distance  $d_{kj}$  (in the  $x$ - $y$  plane) between the predicted position  $(\hat{x}, \hat{y})$  of track  $k$ , and the  $j$ -th candidate observation  $(x_j, y_j)$ , is computed using [27]:

$$d_{kj} = \frac{(\hat{x} - x_j)^2}{\sigma_x^2} + \frac{(\hat{y} - y_j)^2}{\sigma_y^2}. \quad (9)$$

This metric is used to find a set of observation-to-track pairs satisfying a closeness criteria (10), which is based on the covariances of both predictions and measurements:

$$d_{kj} < 3\sqrt{\sigma_{o_x}^2 + \sigma_{o_y}^2 + \sigma_{p_x}^2 + \sigma_{p_y}^2}, \quad (10)$$

where  $(\sigma_{o_x}^2, \sigma_{o_y}^2)$  are the variances of the observations in  $x$  and  $y$ , respectively as in the covariance matrix  $R$  (3); and  $(\sigma_{p_x}^2, \sigma_{p_y}^2)$  are the variances of predictions in  $x$  and  $y$  obtained from the covariance matrix  $\mathbf{P}$ .

Those observations satisfying the closeness criteria are the final candidates for association with track  $k$ . A Global Nearest-Neighbour (GNN) association method, also known as single hypothesis tracking (SHT), is used for its good performance for widely spread targets [27]. The GNN approach, using the normalized distance  $d_{kj}$  in (9) as a cost function, makes a global and optimum decision by considering all pairings combinations together. At the end, GNN assigns only one observation to a given track, and that observation can only be used once.

Finally, all observations-to-track associations are used to update the state of each track,  $\mathbf{a}_{ii}$ , as presented in last subsection using the Kalman filter expression (7). This state update only includes the target's XYZ location and velocity. However, after this state update, other variables of interest for navigation are computed (but not by Kalman filtering) based on the current state or some features of the patterns feeding a target. For example, the heading of the target and its heading's rate of change are estimated; also the size of the target in terms of length, depth and height based on the size of the patterns setting up a target. The total set of estimated parameters, which correspond to those shown in the tests of figure 9, are:

- *Pose*: Target location and heading.
- *Course*: Target velocity and heading's rate of change.
- *Size*: The length, depth and height of the target along  $x$ ,  $y$  and  $z$  axis, respectively.
- *Persistence* ( $\gamma$ ): Score function that reflects the stability of observed patterns feeding a track.
- *Number of components* ( $\eta$ ): Number of single tracks aggregated because they belong to the same object.

For their importance, the strategy used to update *Persistence* ( $\gamma$ ) and the *Number of components* ( $\eta$ ) will be treated in detail in next two subsections.

#### D. Track maintenance

In principle, when a new observed pattern can not be associated to any existing track, then a new track should be initialized [36]. To limit the creation of new tracks from unreliable laser reflections (clutter), basic strategies are typically used such as the  $M/N$  ad-hoc rule, which requires an observation to be present in at least  $N$  of  $M$  consecutive frames ( $M > N$ ), before it can be confirmed as a valid new track. We use the sequential probability ratio test (SPRT) [27], [37] to decide if new tentative tracks should be confirmed, or some old tracks should be deleted.

The idea in track maintenance is to require a pattern to be persistent during several consecutive frames (evaluation phase), before considering it as a valid one. During this evaluation phase we create a temporal virtual track to verify the correctness of next associations with new patterns, but virtual tracks are still not considered as certain until the persistence score function does not reach a given upper threshold. The *persistence* score function is defined recursively [27] as follows:

$$\gamma_i = \gamma_{i-1} + \Delta\gamma_i \quad (11)$$

$$\Delta\gamma_i = \ln \left[ \frac{P_D}{P_{FA}\sqrt{|S|}} \right] - \frac{\ln(2\pi) + d_{kj}^2}{2}, \quad (12)$$

where  $\Delta\gamma_i$  depends on application-dependent parameters, such as the probability of correct detection,  $P_D$ , the probability of false alarm,  $P_{FA}$ , the normalized distance between track  $k$  and observation  $j$ ,  $d_{kj}$  (9), and also on the residual covariance matrix  $S$  defined as  $S = \mathbf{H}\mathbf{P}\mathbf{H}' + R$ , which uses some of the previously defined Kalman matrixes:  $\mathbf{H}$ ,  $\mathbf{P}$  and  $R$ .

We use three thresholds on the persistence score function, to declare three regions where a track should be confirmed, deleted, or continue as as a virtual track under evaluation.

$$\gamma_i = \begin{cases} = T2 & ; \text{track confirmation} \\ > T1 \text{ and } < T2 & ; \text{track evaluation} \\ \leq T1 & ; \text{delete track.} \end{cases} \quad (13)$$

Threshold values are selected using SPRT formulation [27], and it is based on the false track confirmation probability,  $\alpha$ ; and the true track deletion probability,  $\beta$ :

$$T2 = \ln[(1 - \beta)/\alpha] \quad ; \quad T1 = \ln[\beta/(1 - \alpha)]. \quad (14)$$

As an illustration, we assume based on conducted tests, that our system can produce (at observation or pattern level) about 200 false alarms per hour ( $N_{FA} = 200$ ); if we can admit a maximum of three false track confirmations per hour ( $N_{FC} = 3$ ), then  $\alpha$  is

$$\alpha = N_{FC}/N_{FA} = 3/200 = 0.015. \quad (15)$$

In order to avoid the elimination of true targets, a small value for  $\beta$  is selected ( $\beta = 0.05$ ). Using these values for  $\alpha$  and  $\beta$ , the thresholds  $T2$  and  $T1$  computed using expressions in equation 14 are approximately 4 and -3 respectively.

When a new non-associated observation appears, its persistence score is initiated with zero ( $\gamma_0=0$ ). For the next frames, if new patterns are associated with the virtual track under evaluation, then persistence is increased using expression in equation 12 (a typical value for this increase is one unit for  $P_D = 0.7$ ,  $P_{FA} = 0.05$  and  $d_{kj} = 1$  meter). Whenever persistence  $\gamma_i$  reaches  $T2$ , the target is definitively considered as a valid one and persistence saturates at that level.

When no patterns are found for correct association with a certain track, the persistence score function is updated with  $\Delta\gamma_i = \ln(1 - P_D)$ , which for a  $P_D = 0.7$  is -1.2, therefore in that cases the persistence score is decreased approximately by one unit. Also, its kinematic state is updated based only on the prediction

equations of Kalman filtering (5). Those tracks that do not match with any observed pattern during a certain time make the persistence value lower than  $T_1$ , and are removed from the system.

The above described initialization and elimination methods are essential in order to filter out all the inconsistencies that actually appear from frame to frame, due to vessel oscillations and vertical gaps in Ladar frames. This initialization and elimination strategy, causes a delay in the initial detection of targets and on their removal, but this delay is not too significant for the default Ladar frame acquisition mode (approximately 3 seconds delay for initialization and elimination).

### E. Clustering of multiple tracks

For several reasons, a single object can end up being represented by several Ladar traces. Fragmented traces are caused by inhomogeneities in the reflectance of an object (i.e. surfaces with different colors, patterns or textures). Additionally, an object with enough height, during a multi-line image acquisition, can generate several traces, one per each smooth Ladar scan line. So, this partitioned trace acquisition causes a significant number of tracks associated to individual fragments of a target.

Our clustering method groups fragmented parts of an object, into a single multi-component track representing the whole entity. The proposed clustering method transforms, for example, several tracks corresponding to small sections of a ship's hull into a single track representing the whole ship.

The criterion for clustering is based on the following parameters: *proximity*, *velocity* and *direction of movement*. A three dimensional feature space is formed with them. We use a variation of the QT (Quality Threshold) clustering algorithm proposed for gene clustering [38]. One advantage of the QT is that it needs no a priori information on the number of clusters, and it is based on choosing a maximum diameter for clusters and a recursive aggregation of closest candidates. We use the normalized Mahalanobis distance between pairs of tracks to aggregate the closest tracks to an initial candidate track within the given cluster size. As an output of the clustering algorithm, the number of components aggregated in a track,  $\eta$ , is used to indicate if we are tracking an elementary track ( $\eta = 1$ ) or a clusterized multi-component one ( $\eta > 1$ ).

## V. TESTS AND RESULTS

In order to evaluate our Ladar system performance, several tests were carried out both in open-sea conditions and on inland waterways. For inland tests, the river Neckar (affluent of Rhine River in Germany) was selected due to the existence of numerous locks, low profile bridges and narrow waterways. As far as Neckar river is not covered by ECDIS, then it was decided to complete part of the experiments on Rhine river (ECDIS coverage downstream Iffezheim lock). The vessel used for inland test was a freighter for general cargo (length/breadth: 100/11 meters). Open-sea test were conducted by several trips between Salamina island and Pireus harbor (Athens, Greece). In this case a small car ferry was used (length/breadth: 50/12 meters).

The Ladar scanner was installed on the bow of both ships, and the MMI was placed on the ship's bridge. A DGPS receiver and an electronic compass were connected to the Ladar system using the VMI. An additional pan and tilt sensor was used below the scanner to know precisely its inclination with respect to the water level. Tests were performed in good visibility conditions. Next subsections present some results about the usefulness of raw Ladar plots in precise maneuvers, the accuracy in measuring bridge heights, how well Ladar traces are integrated with ECDIS, and target tracking performance.

### A. Precise navigation using raw Ladar images

Direct use of *raw* Ladar information (only Ladar traces, but not ECDIS displaying nor tracking processing) is quite valuable for navigation under the supervision of a skipper for example in rivers like Neckar, which have many locks, suffer heavy traffic of vessels, and have narrow passageways between bridge columns. The Ladar system provides precise ranging information with full ranging coverage (from 1 meter to its maximum range), and therefore can be used to assist the skipper in guiding the vessel along narrow passages in locks and bridges. Two kind of experiments were performed: Entering into a lock chamber with a cargo ship, and measuring the height of some bridges before passing them.

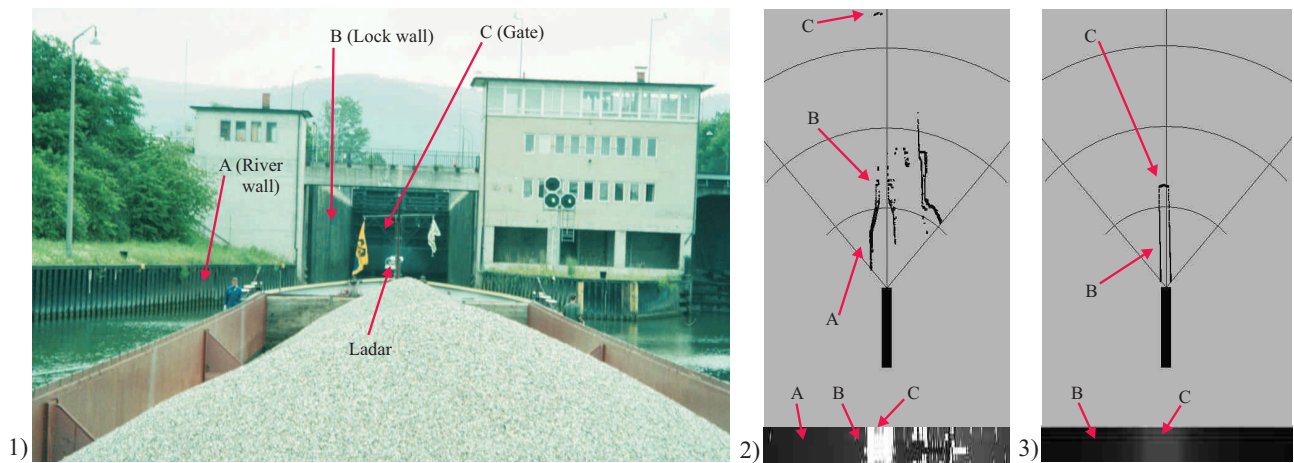


Fig. 6. Entering a lock chamber (length/width: 250/15 meters) at river Neckar. (1) Photograph while approaching the lock; (2) a raw Ladar representation at 100 meters from the entrance to the lock; (3) another raw Ladar display when the bow of the ship is in the middle of the lock chamber at 125 meters from the rear lock gate. At the bottom of Ladar displays in 2 and 3, it is represented the Ladar image (azimuth-elevation vs range) where range is coded using a gray-level colormap (white: no range reading; light-gray: large ranges; dark-gray: short ranges).

1) *Entering into a lock chamber:* Image to the left in figure 6 shows our cargo ship approaching a lock chamber (Schwabenheim lock, Neckar km 17.5). Ladar traces in plot 2 of this figure, make possible the correct alignment of the ship with respect to the lock walls, which is the most critical action during locking. Plot 3 shows how half of the ship is already in the chamber with correct orientation; the shape of lock chamber is precisely sketched, including the rear gate. The accuracy of range traces were in accordance with the ranging unit, about 10 cm accuracy. As the tolerance between the lateral ship's hull and the lock's walls is above 1 meter at both sides, then we believe that Ladar processing and control algorithms could be used to automatically guide a ship into the lock, although factors as the intensity of river's stream-flow can make the task non-trivial.

2) *Estimating bridge heights:* Several bridges in river Neckar were scanned to evaluate Ladar accuracy in estimating clearances (height from lower section of a bridge to water level). The scanner was tilted 90 degrees to perform a vertical fast scanning with the maximum angular resolution. Clearance is estimated using expression:  $C = h_0 + r \cdot \sin(\phi) \cdot \cos(\theta)$ , where  $C$  is clearance,  $r$  is range,  $\phi$  is the elevation angle,  $\theta$  is the azimuth angle, and  $h_0$  is the vertical distance between the water level and the Ladar on the bow. Figure 7 shows a sequence of height estimations while the cargo is approaching a road bridge (in Gernersheim, Germany). Note how at large distances (300 m), the height estimations are less stable due to some remaining uncompensated oscillations, the larger spot diameter, and lower height resolution. At 150 meters or less, estimations become quite repetitive (mean height 6.75 m;  $\sigma=0.08$  m). For our cargo vessel,  $h_0$  is 3.2 meters, therefore clearance  $C$  is 9.95 m, quite close to the actual height value 9.82 meters. Other tests draw similar results indicating a reliable decimeter-level precision.

### B. Overlaying Ladar on ECDIS

In order to improve the interpretation and the graphical presentation of Ladar traces, we overlaid an electronic chart display (ECDIS) color map over the raw Ladar representation (including the ranging Ladar traces, the scanning sector, and the ship outline). The ECDIS-Ladar matching operation was made possible estimating the ship location and orientation with high accuracy. Location information was obtained from a DGPS receiver using WAAS differential corrections with location errors in static conditions of about 2.5 meters. In dynamic operation (vessel in navigation), we found some delays between the DGPS output and the real positioning due to the internal filtering at the GPS receiver. It caused an additional error proportional to ship speed, along the direction of movement, which in our tests was about 4 meters (at 22.5 km/h). The main source of matching errors was the estimation of the orientation. Using the electronic

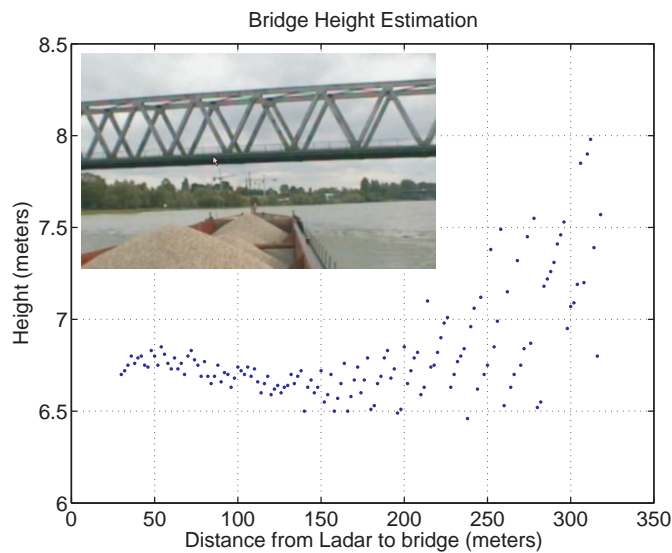


Fig. 7. Bridge height estimations as a function of the distance between the scanner and this bridge. The Ladar scanner was oriented with the fast scanning vertically to obtain good angular/height resolution. A pan and tilt sensor was used to decouple height measurements from ship oscillations.

gyro-compass the matching was unreliable (errors above 5 degrees), so we have to integrate the heading estimation coming from the DGPS, which at speeds above 4 km/h, was much more reliable than the compass alone.

With the above considerations, final matching results were even better than expected, existing a direct correspondence between Ladar traces and objects of interest. Good overlaying occurs in bridge columns, river banks, port layout, etc. Figure 8 shows a ship approaching a bridge in river Rhine. Blue-shaded colors represent the water mainstream, while brown colors the terrain. The intensity of colors represent the depth or height (for blue and brown colors, respectively) referred to the water level. A bypassing ship is detected at the left-hand side (trace A). It can be seen that the columns of bridges (traces B and C) are easily detected and matched to the ECDIS charts. The left-hand column is not detected because is occluded by the by-passing ship.

### C. Tracking obstacles

Target tracking tests were conducted in a small car ferry in Athens (Greece). We checked the robustness of tracking with cluttered and fragmented Ladar profiles. Results show how individual tracks with similar properties are clustered together into high level targets. Figure 9 presents a list of tracks generated during a trip between the Pireus harbor in Athens and the Salamis Island. In this track list, small targets such as '12', '19', '48' and '51' are detected. Additionally, many broken segments are grouped together in multi-component tracks of bigger size such as '1', '2' and '7' which are clusters of 5, 5 and 3 simple tracks, respectively.

Figure 10 shows a snapshot of a travel between Salamis Island and Pireus harbour. Two targets are detected, an approaching ship at 150 m distance on the left-hand side, and a small vessel in front of us with almost the same course. A visual representation of their position and size estimations is done by overlaying small squares on top of the detected objects.

Details of the filtering properties of Kalman estimation for a sequence of 84 consecutive Ladar frames are presented in figure 11. Figure 11(left) plots the position in the  $x-y$  plane of observations and subsequent-formed tracks, and figure 11(right) shows the persistence score for those tracks when the valid track range is between 0 and 3. Two significant observations are detected since the beginning of tracking (observations 1 and 2 in red and black colors, respectively), and consequently two tracks are confirmed and maintained;

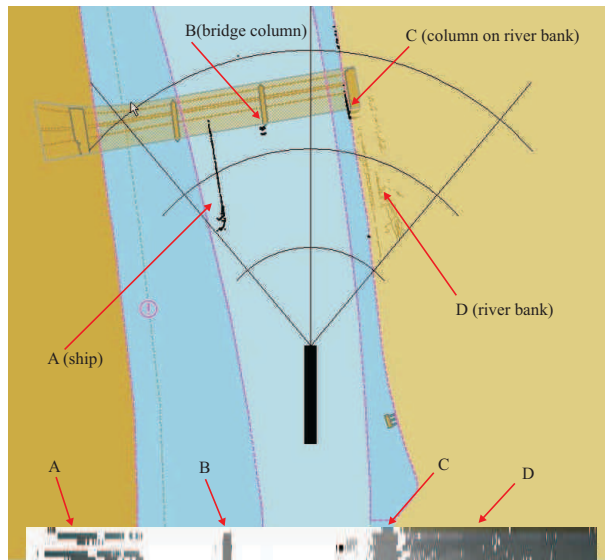


Fig. 8. Integration of ECDIS map with Ladar scans (black traces), during an in-land operation approaching a bridge in river Rhine. DGPS positioning and orientation is used for correctly matching ship/Ladar data onto the electronic map. Note that the three radar black traces from left to right correspond to: A) an approaching vessel, B) the central bridge column, and C) the right-hand river bank. Label D) represents detections on right-hand river bank.

Label	Persistence	Number of Components	Pose				Course					Size	Confidence	Time Code		
			Dist	X	Y	Z	heading	V	Vx	Vy	Vz				Vheading	
1	2.8	5	102.6	-31.2	97.7	-0.0	0.5	1.0	-0.1	0.9	-0.0	0.0	44.0	81.0	1.0	111650
2	3.0	5	48.4	0.2	48.4	-0.0	-0.1	0.2	0.2	0.0	-0.0	0.0	25.5	4.2	1.0	111650
3	3.0	2	195.2	35.2	192.0	-0.0	0.8	1.0	1.0	-0.2	0.0	0.0	40.4	3.7	1.0	111650
5	3.0	2	267.2	113.7	241.8	-0.0	0.3	3.4	3.3	-0.8	-0.0	0.0	62.0	5.3	1.0	111650
7	3.0	3	145.9	-3.1	145.9	-0.0	0.9	0.9	0.8	-0.6	0.0	0.0	33.8	7.5	1.0	111650
12	3.0	1	240.3	20.2	239.4	-0.0	-0.8	2.6	2.6	-0.4	0.0	0.0	3.4	0.0	1.0	111650
19	3.0	1	261.1	13.9	260.7	-0.0	-0.9	2.1	2.0	-0.7	0.0	0.0	7.3	0.0	1.0	111650
39	3.0	2	100.0	-10.2	99.5	-0.0	-0.6	0.7	0.6	0.3	-0.0	0.0	7.2	0.2	1.0	111650
40	1.5	2	173.9	0.3	173.9	-0.0	0.5	0.4	-0.2	-0.4	0.0	0.0	9.3	1.8	1.0	111650
48	3.0	1	103.7	-50.1	90.8	-0.0	-0.4	3.0	-2.8	1.0	-0.0	0.0	2.3	0.0	1.0	111650
50	1.5	2	252.8	69.5	243.1	-0.0	0.1	0.8	0.7	-0.3	-0.0	0.0	10.5	0.0	1.0	111650
51	0.0	1	342.2	194.3	281.6	-0.0	0.0	0.0	0.0	0.0	0.0	0.0	0.2	0.0	1.0	111650

Fig. 9. A sample track list corresponding to a situation during a trip between Pireus harbor in Athens and Salamis Island

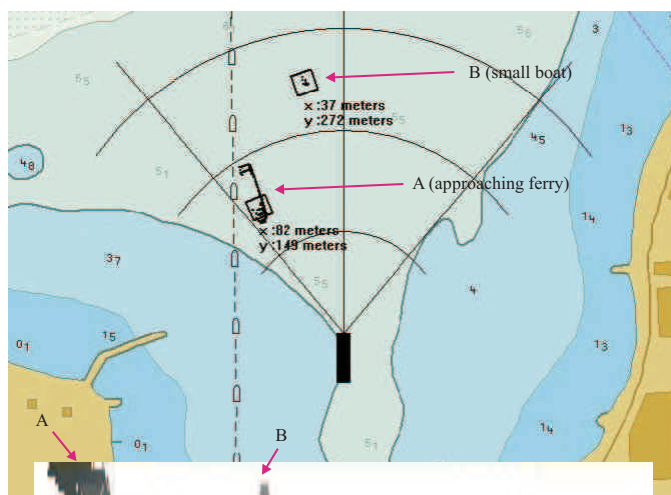


Fig. 10. Target tracking estimation in the middle of a travel between Salamis Island and Pireus harbour, Athens (Greece). Two multi-component tracks are created which correctly correspond to an approaching ferry (left-hand side) and a small boat in navigation with our same course (in front of us).

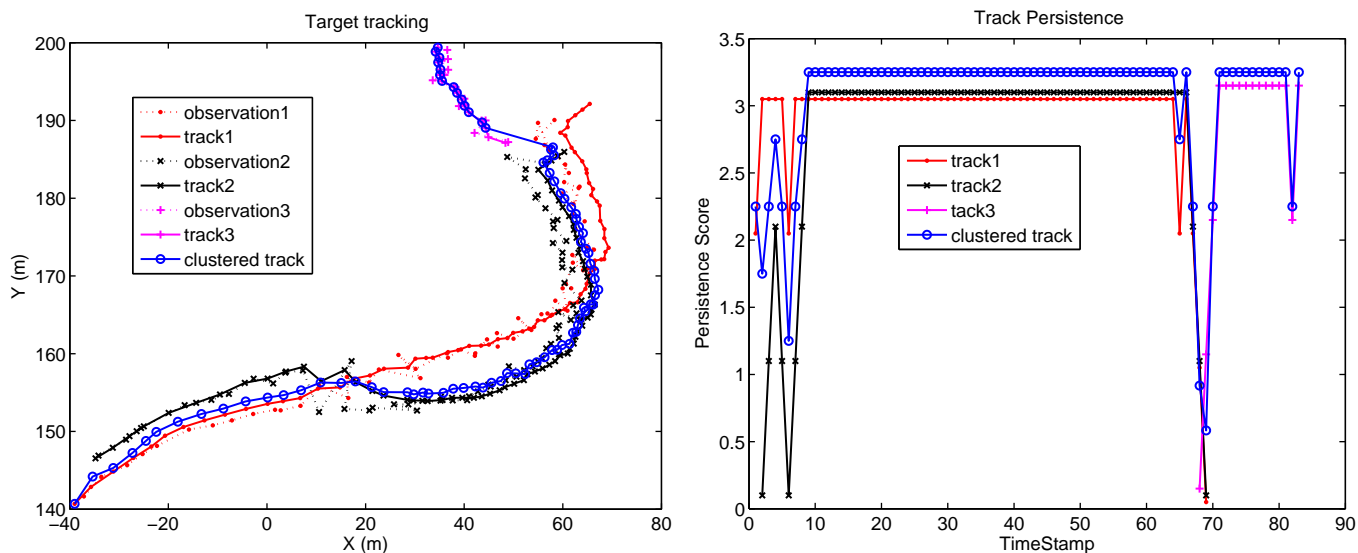


Fig. 11. Target tracking sequence for a small vessel in front of our ship: (left) Several observations for the vessel hull, tracks after Kalman filtering, and integration of individual tracks on a multi-component track representing that vessel; (right) Persistence score function for those tracks vs time.

but after a stable behavior lasting more than 50 consecutive frames, observations 1 and 2 are lost during several consecutive frames (see decrease in persistence score starting at time-stamp 65). Before the end of the sequence, a third observation becomes persistent starting at frame number 70 (observation 3 in magenta) creating track number 3. These individual tracks are fused together into a multi-component track whose parameters are a weighted average of individual tracks. Note that the clustered multi-component track is insensitive to the transition from tracks 1-2 to track 3, and keeps a continuous estimation with a persistence above zero all the time.

## VI. DISCUSSION

Our Ladar system is capable of detecting many objects of interest, which it is essential to achieve the challenging goal of precise maneuvering, fluent navigation and accident mitigation. Nearby boats and ships are clearly detected at distances up to 400 meters. Vessels ranging from small boats to large ships are detected, and even buoys can be perceived intermittently in some frames. The pier and the lock chamber outlines can be precisely sketched, making possible for the skipper to rely on Ladar information for berthing or entering the lock. Inland waterways are also clearly defined; and the integration of Ladar data, GPS and ECDIS maps is completely achieved, making possible an efficient interpretation of navigation conditions. For example, using horizontal fast scanning, the columns of bridges are reliably detected, and correctly matched to corresponding ECDIS objects.

Bridge clearance estimation is essential for inland waterways, because water level can change significantly in a few hours time, increasing the risk of collisions with bridges. The combination of the pan and tilt sensor with the Ladar in vertical scanning has been very useful to precisely estimate the elevation angle to the lower section of a bridge. Bridge clearances were estimated, as described in the result section, with decimeter accuracy.

Pan and tilt sensing, however, can not be used to make Ladar frames independent from ship oscillations (pitch and roll). The significant inter-line gaps (3 degrees for default mode), makes not feasible the reconstruction of images to become inclination independent. This reconstruction could be done using high density images in both elevation and azimuth axes, but with current Ladar technology this dense scanning requires many seconds to be completed, and therefore, it is not a practical solution. Fortunately, low-amplitude ship oscillations are not a drawback at all, because they help to better detect objects laying between the existing inter-line gaps. However, when the movement of the vessel is too intense (rough

water or small ships), then it might be essential to use an active stabilization platform to level the Ladar scanner.

Some limitations of the Ladar system were identified, related to the maximum range achievable for open sea navigation, which was about five hundred meters shorter than original specifications. This restriction is important for large or fast moving ships, that need a significant amount of time to manoeuvre. Improvement of maximum ranging, should be explored by using lasers with wavelength above 1500 nm. This technology is not yet mature enough for long range ranging, but has the great advantage of making possible the use of higher output laser power since eye-safety restrictions do not apply at those wavelengths. Additionally, a better performance would be desirable in frame update frequency. A faster image acquisition would reduce time delays between perception and action, and would provide more redundant information for further robustness.

Filtering of raw Ladar range profiles, has proved to be very useful to clear out noise and to refine observations. Some artifacts that have been sporadically observed are: 1) specular reflections from the water surface (only when water is dead calm), 2) direct echoes from foam-crested waves, and 3) reflections from very dirty water or with a significant amount of floating debris. Specular reflections on calm water (no light scattered back to ranging unit) deflect laser beam upwards increasing the probability to hit an object of interest; therefore calm water reflections are beneficial to improve scanning efficiency.

The importance of correctly initiating or modifying a maneuver for collision avoidance (either under skipper supervision or automatically) based on the processed Ladar data, makes critical the requirements for robust interpretation, which should specially minimize false alarms while maximizing the probability of detection of true threats. This fact justifies the need for several levels of redundancy and consistency, as proposed in this paper, where an outlier minimization stage with order filtering techniques (section IV-A), is followed by robust target tracking initialization and elimination strategies (section IV-D).

## VII. CONCLUSIONS

A new maritime navigation system based on a laser range-finder scanner has been described in this paper. The main novelty of this work is the adaptation and implementation of known technology for laser range-finding and algorithms for target tracking, into a system that operates in real-time and has been tested in different natural sea and in-land navigation scenarios. The prototype developed can be considered as a very valuable complementary device to traditional radar-based techniques, that are not valid for accurate short-range exploration, to improve efficiency and safety in ship operations.

Along this paper we have described the Ladar navigation system and the algorithms implemented for target identification and tracking. After presenting the motivation of this project, we described in detail the principal components of the system: the laser range-finder, the scanning unit, the data processing (pattern identification and target tracking), and the graphical MMI unit. We proposed to employ laser telemetry in a real-time application problem. Although the image density is limited by a maximum rate of 15,000 range values per second, we defined a configurable field-of-view image acquisition, which, in the default acquisition mode, captures 1500 point per horizontal line, and it is sparse vertically. Our acquisition design is a compromise between capturing the significant features of the scene and, at the same time, acquiring and processing images in real-time. After the raw range scans were captured, images were processed for outlier removal and features-of-interest extraction. A robust strategy was introduced to achieve a continuous tracking of significant features, minimizing unreliable track initializations and preserving tracks during temporal mis-observations. A traditional Kalman filter was used for each target under track, in a multi-target tracking approach.

The system was evaluated in open-sea (Pireus-Salamina trips) and in-land waterways (Neckar and Rhine river). Different scenarios were selected for tests: entering the port and pier, open-sea navigation, approaching bridges and locks, measuring bridge heights, and crossing other vessels in narrow inland waterways. Some of the results obtained in reliable object-of-interest detection and tracking, make our Ladar system a very valuable instrument for precise maneuvering, fluent navigation and accident mitigation. Also, some

limitations (regarding maximum ranging achieved, frame acquisition time, and oscillation-independent imaging), were discussed and some research directions were pointed out for future improvements.

We envision a near future where short-range sensors, such as the one presented in this paper, will be installed in vessels to achieve the safety and efficiency demanded in sea transportation systems. The ultimate goal would be to have an on-board computer taking control of the ship in emergency situations (avoid a collision) or commanding the ship while performing delicate manoeuvres. To achieve this goal, further investigation in this direction is needed, specially in the field of real-time range imaging, but also on robust data interpretation, and decision-making. Nevertheless, the proposed methodology can already complement radar, GPS and ECDIS systems, in order to trigger alarms when a collision risk is detected, or as an improved representation for the skipper.

## REFERENCES

- [1] E. Olsson and A. Jansson, "Work on the bridge: Studies of officers on high-speed ferries," *Behaviour & Information Technology*, vol. 25, no. 1, pp. 37-64, 2006.
- [2] M. Nielsen and J. Petersen, "Collision Avoidance at sea - Practice and Problems," in *Proceedings of 20th European Annual Conference on Human Decision Making and Manual Control*, June 2001, pp. 81-90.
- [3] R. Wawruch, J. Cydejeko and M. Dziewicki, "Testing the quality of information on tracked vessels in a VTS centre with GNSS," *Journal of Navigation*, vol. 52, pp. 252-258, 1999.
- [4] B. Zigic and J. Suomela, "The short range navigation, positioning and obstacle avoidance system," in *Int. Conf. SURV V Surveillance, Pilot and Rescue Craft, Southampton*, May 2000, pp. 1-11.
- [5] N. Kjerstad, "Low cost radar surveillance system", *European Journal of Navigation*, vol. 2, no. 2, pp. 9-14, May 2004.
- [6] M.I. Skolnik, *Introduction to Radar systems*, McGraw-hill, 2002.
- [7] F.L. Chevalier, *Principles of Radar and Sonar Signal Processing*, Artech House, 2002.
- [8] R.J. Mailloux, *Phased array antenna handbook*, Artech House, 1994.
- [9] A. Kochan, "Radar is set to revolutionise road safety," *Sensor Review*, vol. 23, no. 2, pp.109-115, 2003.
- [10] K. Schuler, M. Younis, R. Lenz and W. Wiesbeck, "Array design for automotive digital beamforming radar system," in *IEEE International Radar Conference*, May 2005, pp. 435- 440.
- [11] R. Abou-Jaoude, "ACC radar sensor technology, test requirements, and test solutions," *IEEE Trans. on Intelligent Transportation Systems*, vol. 4, no. 3, pp. 115-122, 2003.
- [12] Y.F.L. Vincent and K.M. Miller, "Target detection in radar: current status and future possibilities," *Journal of Navigation*, vol. 50, pp. 303-313, 1997.
- [13] D.C. Carmer and L.M. Peterson, "Laser radar in robotics," in *Proceedings of the IEEE*, vol. 84, no. 2, pp. 299-320, Feb. 1996.
- [14] M. Juberts and A. Barbera, "Status report on next generation LADAR for driving unmanned ground vehicles," in *Proceedings of SPIE Mobile Robots XVII Conf.*, vol. 5609, 2004.
- [15] J.S. Accetta, *The infrared and electro-optical systems handbook*, SPIE Pres, 1993.
- [16] T. Makinen, *Requirements for Preventive Safety Applications*, Report of E.U. Project number FP6-507075 in the eSafety for road and air transport program, 2005.
- [17] M. Parent, "Automated urban vehicles: state of the art and future directions," in *Control, Automation, Robotics and Vision Conference*, vol. 1, 2004, pp. 138-142.
- [18] R. Behringer, B. Gregory, V.Sundareswaran, R. Addison, R. Elsley, W. Guthmiller, J. deMarchi, R. Daily, D. Bevely and C. Reinhart, "Development of an autonomous vehicle for the DARPA Grand Challenge", in *IEEE Intelligent Vehicles Symposium*, June 2004, pp. 226-231.
- [19] B. Zigic, *Problem characterisation in Shico project*, Report of Brite/Euram-Craft E.U. project number BE-ST-2871, June 1999.
- [20] Y. Bar-Shalom and X. Li, *Estimation and Tracking Techniques*, YBS, 1998.
- [21] E. Brookner, *Tracking and Kalman Filtering made easy*, Wiley-Interscience, NY, 1998.
- [22] H. Weichel, *Laser Beam Propagation in the Atmosphere*, SPIE, Bellingham WA, 1990.
- [23] J.M. Wallace and P.V. Hobbs, *Atmospheric Science: An Introductory survey*, Academic Press, Orlando, 1977.
- [24] E.J. McCartney, *Optics of the Atmosphere*, J. Wiley & Sons, New York, 1976.
- [25] V.J. Fowler and J. Schlafer, "A survey of laser beam deflection techniques", in *Proceedings of the IEEE*, vol. 54, no. 10, 1966, pp. 1437-1444.
- [26] Y. Li and J. Katz, "Laser beam scanning by rotary mirrors: Modeling mirror-scanning devices," *Applied Optics*, vol. 34, pp. 6403-10, 1995.
- [27] S. Blackman and R. Popoli, *Design and analysis of modern tracking systems*, Artech House, 1999.
- [28] D. Bruza, and Th.P. van der Weide, "The Semantics of Data Flow Diagrams", in *Proceedings of the International Conference on Management of Data*, pp. 66-78, 1989.
- [29] P.J. Huber, *Robust Statistics*, Wiley, N. Y., 1981.
- [30] P.J. Rousseeuw and A.M. Leroy, *Robust Regression and Outlier Detection*, Wiley, N.Y., 1987.
- [31] V. Barnett and T. Lewis, *Outliers in Statistical Data*, Wiley, N. Y., 1994.
- [32] S.C. Chan, Z. Zhang and K.W. Tse, "A New Robust Kalman Filter Algorithm under outliers and System Uncertainties," in *Proc. of IEEE Int. Symposium on Circuits and Systems*, 2005, pp.4317-4320.

- [33] J. Canny, "A computational approach to edge detection," *IEEE Trans on Pattern Analysis and Machine Intelligence*, vol. 8, no. 6, pp. 679-698, 1986.
- [34] Y. Bar-Shalom and E. Tse, "Tracking in a cluttered environment with probabilistic data association", in *Proc. of the 4th Symposium on nonlinear estimation theory and its applications*, 1974.
- [35] F. Folster, H. Rohling, "Data association and tracking for automotive radar networks," *IEEE Transactions on Intelligent Transportation Systems*, vol. 6, no. 4, pp. 370-377, 2005.
- [36] H. Gauvrit, J.P.L. Cadre and C. Jauffret, "A formulation of multi-target tracking as an incomplete data problem," *IEEE Trans. on Aerospace and Electronic systems*, vol. 33, no. 4, 1997.
- [37] C. Coué, T. Fraichard, P. Bessiere and E. Mazer, "Using Bayesian programming for multi-sensor multi-target tracking in automotive applications," in *Proc. of the IEEE Int. Conf. on Robotics and Automation*, May 2003.
- [38] L.J. Heyer, S. Kruglyak and S. Yooseph, "Exploring Expression Data: Identification and Analysis of Coexpressed Genes," *Genome Research*, vol. 9, pp. 1106-1115, 1999.